Crystal symmetry in single domains of $PbZr_{0.54}Ti_{0.46}O_3$

Roland Schierholz* and Hartmut Fuess
Institut für Materialwissenschaft, Technische Universität Darmstadt, 64827 Darmstadt, Germany

Kenji Tsuda, Yoishiro Ogata, and Masami Terauchi
IMRAM, Tohoku University, Sendai, Japan

Ralf Theissmann
Institut für Nanostrukturtechnik, Universität Duisburg-Essen, Duisburg, Germany

(Received 25 April 2008; revised manuscript received 20 June 2008; published 29 July 2008)

This work focuses on the crystal symmetry of morphotropic $PbZr_xTi_{1-x}O_3$ (PZT). The crystal symmetry is investigated within single domains of ≈30–100 nm width by convergent beam electron diffraction (CBED). The composition $PbZr_{0.54}Ti_{0.46}O_3$ was chosen for experiments at room temperature and ≈300 °C. The observed zone axis symmetry at room temperature was a $(\bar{1}10)$ mirror in some domains whereas symmetry was broken in neighboring domains. Therefore the highest crystal symmetry that can be attributed with certainty to the probed volume is monoclinic. The local symmetry of single cells might be lower due to disordered displacements of the cations. At ≈300 °C the zone axis symmetry had changed to a $(100)_{pc}$ mirror that only occurs in the tetragonal phase of PZT.

DOI: 10.1103/PhysRevB.78.024118 PACS number(s): 61.05.jm

I. INTRODUCTION

The solid solution of $PbZr_xTi_{1-x}O_3$ (PZT) is of technological interest due to its excellent electromechanical properties.[1] The maximum value of the piezoelectric coefficient is observed close to the morphotropic phase boundary (MPB) at a composition of $x/(1-x) \approx 52/48$. Jaffe *et al.*[2] defined the MPB as the line of coexistence of a rhombohedral and a tetragonal phase of equal fractions. The crystal symmetry changes from rhombohedral for zirconia rich compositions to tetragonal for a higher titania content. Also, transitions from rhombohedral to tetragonal were reported for morphotropic compositions with increasing temperature.[3] With samples prepared by semiwet route, the coexistence region was as narrow as $\Delta x = 0.01$. The correlated measurements of the planar electromechanical coefficient showed the maximum for samples that were identified to be tetragonal by x-ray powder diffraction (XRPD). Therefore the high polarizability should rather be caused by lattice softening than by the coexistence of the ferroelectric rhombohedral (F_R) and the ferroelectric tetragonal phase (F_T).[3]

Based on additional reflections observed in high resolution (XRPD), Noheda *et al.*[4] proposed a monoclinic structure for the MPB region. Since *Cm* is a subgroup of *R*3*m* and *P*4*mm*, this is a reasonable symmetry for an intermediate phase connecting tetragonal and rhombohedral phases via a common mirror plane. In their model, already in the tetragonal phase, lead is shifted away about ≈0.2 Å from (0,0,0) to $(x,x,0)$ with local disorder resulting in anisotropic displacement factors. The monoclinic phase is then formed by ordering of lead shifts. For rhombohedral PZT additional lead shifts in $\langle 100 \rangle_{pc}$ were introduced by Corker *et al.*[5] Thus the ferroelectric monoclinic phase (F_M) could be reached from both, rhombohedral and tetragonal side of the phase diagram, by ordering of additional lead displacements.[6] This results in a rotation of the polarization direction from $[001]_{pc}$ to $[111]_{pc}$ within the $(\bar{1}10)_{pc}$ mirror plane. Nevertheless, Glazer *et al.*[6] state that the order/disorder behavior is responsible for the high piezoactivity rather than the rotation of the polarization.

The stability region of the monoclinic phase was defined in a subsequent work for compositions $0.51 \leq x \leq 0.54$ (Ref. 7) in samples prepared from mixed oxides. The highest monoclinic distortion at room temperature was reported for $PbZr_{0.54}Ti_{0.46}O_3$. Therefore the present contribution concentrates on this composition. The slope of the MPB in the $PbZrO_3$-$PbTiO_3$ phase diagram implies a coexistence of tetragonal and monoclinic phases due to compositional fluctuations in samples prepared by solid-state reaction.[4] Above ≈175 °C the material should be tetragonal and turn cubic at the *Curie* temperature of ≈387 °C.[7] For higher titania content the F_M to F_T transition temperature decreases strongly and the monoclinic phase becomes only stable below room temperature. The composition $PbZr_{0.55}Ti_{0.45}O_3$ is already reported to be rhombohedral. So the F_M-F_R phase boundary is supposed to be a vertical line, because no F_M-F_R transition was observed with temperature.[7] Raman spectroscopy[8,9] also showed the stability of the monoclinic phase within the MPB region and a quasivertical F_M-F_R boundary. Pandey[10] and Singh[11] doubt the existence of this phase boundary and extend the stability region of the Cm phase which behaves pseudorhombohedral for higher zirconia content.

Recent studies showed that the influence of domains and domain walls in the material on structural investigations by scattering techniques should not be neglected. Schmitt *et al.*[12] gave an overview on domain sizes over the MPB. Around the MPB domain, size increases but also nanodomains occur. These are the compositions that show the additional reflection in XRPD attributed to monoclinic phase by Noheda.[13] Because of this coincidence the reflection may be attributed to coherence effects.[14]

Wang[15,16] explained the adaptive reflection by diffraction theory. According to this approach, coherent diffraction of

several rhombohedral nanodomains produces a reflection similar to one of a monoclinic phase of type M_A,[17] with polarization along $[uuw]$ and $u \leq w$. With tetragonal nanodomains, this model leads to an adaptive reflection according to monoclinic phases M_B and M_C,[18] with polarization in $[uuw]$ (M_B) but $u \geq w$ or polarization in $[0uv]$.[17] Such structures were proposed for intermediate phases in PMN-PT $(Pb(Mg_{1/3}Nb_{2/3})_{1-x}Ti_x$.[19] In a study on PMN-PT, Wang *et al.*[20] observed tetragonal symmetry in nanodomains ≤ 10 nm by convergent beam electron diffraction (CBED), using a field-emission gun (FEG) and spot size of 2.4 nm. Wang *et al.* propose an easy rearrangement of the nanodomains in an electric field. For morphotropic PZT *in situ* electric field x-ray diffraction and transmission electron microscopy (TEM) experiments demonstrated a reaction of nanodomains.[21,22] Therefore it may be stated that the nanodomains increase the reaction of the material.

In the present work we attempt to determine the crystal symmetry of single domains in $PbZr_{0.54}Ti_{0.46}O_3$ by CBED to exclude coherence effects. An additional heating experiment is performed to detect phase transitions caused by heating above the MPB.

II. EXPERIMENTAL PROCEDURE

A. Sample preparation

The material with composition $PbZr_{0.54}Ti_{0.46}O_3$ was processed using the mixed oxide route.[23] Pellets were pressed and sintered at 1050 °C for 6 h. The ceramic was cut by a wire saw and ground down and polished to the dimensions $2.5 \times 2.5 \times 0.1$ mm^2. Subsequently the samples were ion milled to electron transparency with a JEOL ion slicer EM-09100IS.[24] The parameters for initial thinning were an accelerating voltage of 6 kV and inclination angle of $2° - 3°$. After 2–3 h the final thinning was carried out with 2–3 kV and an inclination angle of 1° for about 10 to 30 min. Two samples *A* and *B* were prepared in this way. Sample *A* was investigated at room temperature with a double tilt holder while sample *B* was investigated at room temperature and $\approx 300 \pm 20$ °C using a double tilt heating stage. The experiments were performed at a JEOL 2010 equipped with LaB_6 cathode operated at 100 kV. For CBED, a spot size of 10 nm was used. As recording material, Fuji Film Image plates (IP's) were used. To avoid contamination, prior to the experiment the sample was cleaned by a plasma cleaner.

B. Symmetry determination

The intensity distribution in CBED patterns is very sensitive to crystal symmetry. In combination with TEM imaging one can pick a single domain for diffraction. According to literature, three structures with little distortion from cubic symmetry have to be considered: tetragonal $(P4mm)$, monoclinic (Cm), and rhombohedral $(R3m)$. Because of the C centering of the monoclinic cell, monoclinic$_m$ indices vary from pseudocubic$_{pc}$, tetragonal$_t$ and rhombohedral$_r$ ones (Fig. 1). The $(\bar{1}10)_{pc}$ mirror plane is present in all structures due to subgroup relations. This is shown in Table I and the stereographic projections in Fig. 1. This compilation also visualizes the directions, which allow a distinction of the three point groups by zone axis symmetry. This is discussed in the subsequent paragraphs.

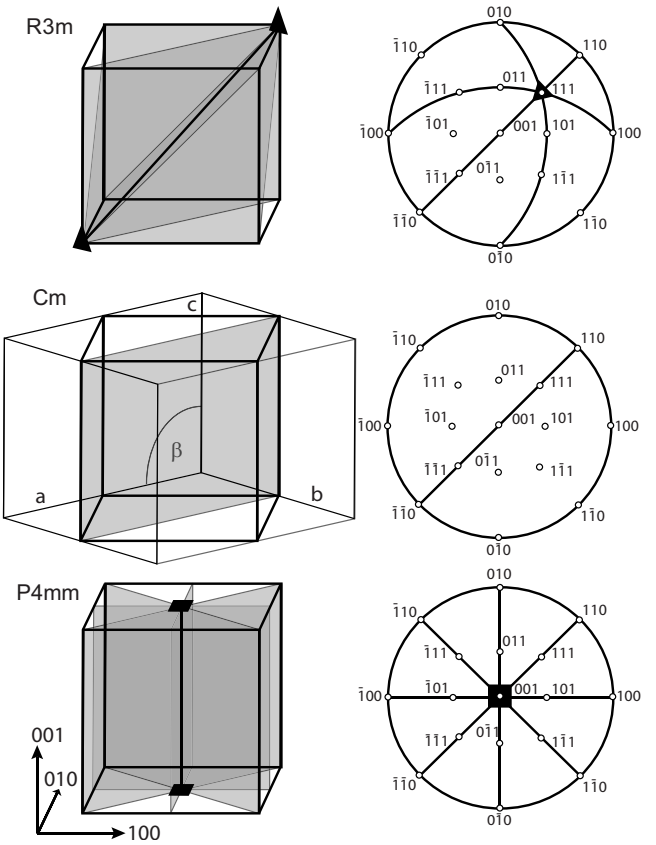

FIG. 1. (a) Unit cells for the three space groups *P*4*mm*, *Cm*, and *R*3*m* with symmetry elements. (b) The mirror planes in stereographic projections along $[001]_{pc}$. Both visualize zone axis symmetries observable with convergent beam electron diffraction (CBED).

1. $\langle 100 \rangle_{pc}$

Tetragonal symmetry can be identified unambiguously in this direction because the zone axis symmetry is $m\{100\}_{pc}$ or 4 mm. In case a $\{110\}_{pc}$ mirror is observed, rhombohedral and monoclinic symmetry have to be considered. In the rhombohedral case all $\langle 100 \rangle_{pc}$ axes have this symmetry. In the monoclinic case the probability for the mirror to occur is $\frac{1}{3}$ while the other two $\langle 100 \rangle_{pc}$ axes have no symmetry. This direction might be found in neighboring domains with different orientations.

2. $\langle 111 \rangle_{pc}$

The threefold axis along $[111]_{pc}$ can identify rhombohedral symmetry. The other three rhombohedral $\langle 1\bar{1}1 \rangle_r$ axes

TABLE I. Zone axis symmetries along pseudocubic zone axes for the three point groups 3*m*, *m*, and 4*mm*.

	3*m*	*m*	4*mm*
$\langle 100 \rangle$	$m\{110\}$	1 or $m\{110\}$	$m\{100\}$ or 4*mm*
$\langle 110 \rangle$	1 or $m\{110\}$	1 or $m\{110\}$	$m\{100\}$ or $m\{110\}$
$\langle 111 \rangle$	$m\{110\}$	1 or $m\{110\}$	$m\{110\}$

reveal a $(\bar{1}10)$ mirror as well as all four tetragonal $\langle 111\rangle_t$ axes. In the monoclinic structure, only half of the $\langle 111\rangle_{pc}$ directions depict this symmetry. In monoclinic settings these are the $\langle 101\rangle_m$ directions while no symmetry is present along $\langle 011\rangle_m$ zone axes.

3. $\langle 110\rangle_{pc}$

$\langle 110\rangle_{pc}$ zone axes can only prove tetragonal symmetry in case of viewing along $\langle 101\rangle_t$. In case of $\langle 110\rangle_t$ the zone axis symmetry is the same that may occur for all structures. Both structures, monoclinic and rhombohedral, also have $\langle 110\rangle_{pc}$ axes without symmetry. So they may not be distinguishable along this direction.

C. Simulations

The simulations of CBED patterns were accomplished using the package MBFIT (Many-Beam dynamical-simulations and least-squares FITting) by Tsuda.[25] In the present work only visual comparison of simulations with the observed results was done. For simulations, the three structures tetragonal, monoclinic, and rhombohedral using lattice parameters and atomic positions published by Noheda *et al.*[4,7] were used. Structural parameters were not refined. Only sample thickness was varied in 5 nm steps.

III. EXPERIMENTAL RESULTS

A. Symmetry at room temperature

Sample *A* was investigated at room temperature. Results for $\langle 100\rangle_{pc}$ and $\langle 111\rangle_{pc}$ zone axes are shown in the following. The area oriented along $[100]_{pc}$ can be seen in Fig. 2(a). Microdomain walls mainly with tracks close to the $[010]_{pc}$ direction are present. Few domain walls with other orientations are observed. Though several domains were investigated, only two are shown in Figs. 2(b) and 2(c) for simplicity. The corresponding beam positions in Fig. 2(a) have been reconstructed from double exposures. In most zone axis patterns (ZAP) no symmetry is present as in the one taken from position 2 shown in Fig. 2(b). This corresponds to one of the four possible $[1\bar{1}0]_m$ directions. The orientation of the *c* axis given in the pattern was chosen according to matching details in the simulated pattern shown in Fig. 2(d).

The interpretation of other patterns sometimes may bear some ambiguity. The intensity distribution is strongly dependent on sample thickness and differences from ideal symmetry can be less pronounced for some thicknesses. According to simulations sample thickness in this area is ranging from about 60–100 nm or above.

The pattern of domain 8 [Fig. 2(c)] is from a ≈110 nm thick area. The intensity distribution of the pattern is close to a $\{1\bar{1}0\}$ mirror plane. This is present looking along $[001]_m$. Since the *c* axis is maintained in the transition from tetragonal to monoclinic after Noheda *et al.*,[13] this direction should occur in this domain configuration. Inclined microdomain walls with tracks in $\langle 100\rangle_{pc}$ are present in tetragonal *a-c* domain configurations.[26]

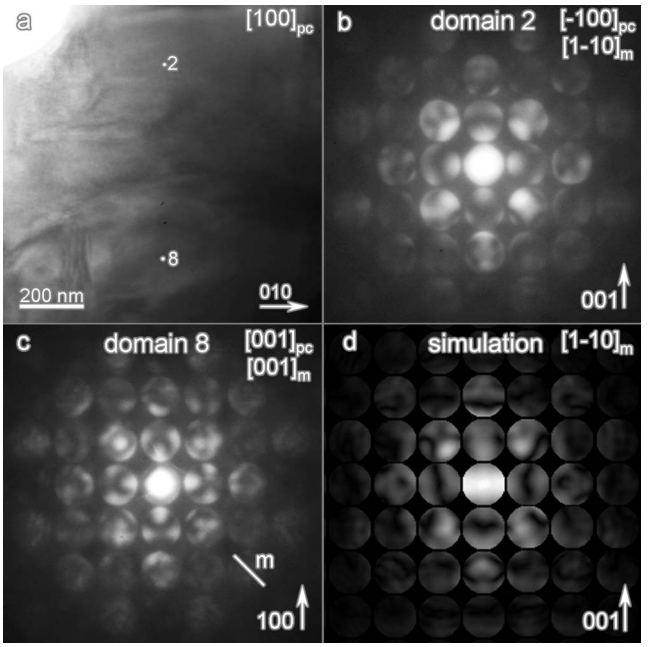

FIG. 2. (a) Image of an $\langle 100\rangle_{pc}$ oriented area in sample *A* at 20 °C. Mainly domain wall with tracks running along [010] are visible with some additional inner domain walls. The spots index the position for convergent beam electron diffraction (CBED) and were reconstructed from double exposures. (b) The $[100]_{pc}$ zone axis pattern (ZAP) of domain 2 shows no symmetry according to $[1\bar{1}0]_m$ orientation. (c) $[100]_{pc}$ ZAP of domain 8 with intensity distribution close to $(1\bar{1}0)$ symmetry. (d) The simulated $[1\bar{1}0]_m$ ZAP with an orientation matching to domain 2 with a sample thickness of 65 nm.

In Fig. 3(a), an area in $\langle 111\rangle_{pc}$ orientation is shown. In the subsequent paragraph it is indexed as $[\bar{1}\bar{1}1]$ to give the orientations of domain walls and domain orientations. The domain configuration mainly consists of two parts. In the left part the domain walls are parallel to the beam. The respective reflection to this plane is $1\bar{1}0_{pc}$. In the right part the domain walls are inclined with traces running close to [011] direction. Therefore, the possible orientation of the domain walls can be either (100) or $(0\bar{1}1)$, if only mirror planes of the parent phase that are not present in the ferroelastic phase[27] are considered as possible domain walls.

From three of these domains diffraction patterns were taken (Fig. 4). The beam positions are shown in Fig. 3(a). The patterns of domain 1 are similar to the patterns of domain 3 and are not shown here. This is consistent with image contrast, which shows an additional domain in between 1 and 3, so they are expected to have the same orientation. Both domains also appear dark due to diffraction contrast in the bright-field (BF) image. Domain 2 appears bright in the BF image [Fig. 3(a)] as well as the domain between 1 and 3. The different orientation of domain 2 is proven by the CBED patterns.

The projected whole pattern (proj. WP), whole pattern (WP) and dark-field pattern (DP) for domain 2 and 3 are shown in Figs. 4 and 5. For domain 3 all patterns reveal a mirror plane in horizontal orientation according to $(011)_{pc}$.

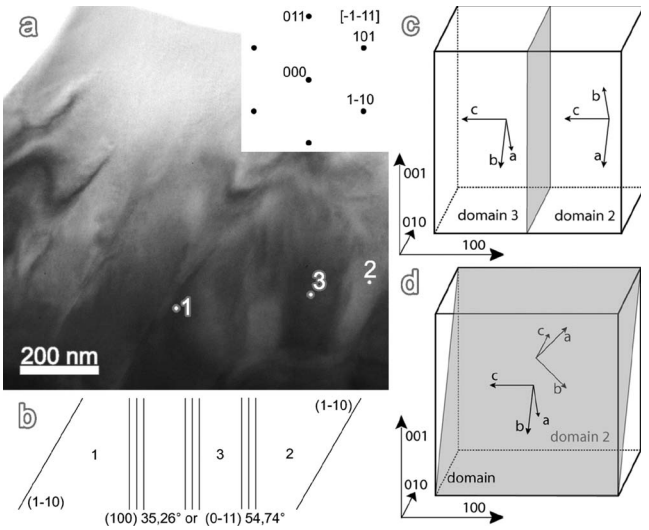

FIG. 3. (a) Bright-field (BF) image of domain configuration in sample *A* viewed along $\langle 111\rangle_{pc}$. The spots correspond to the positions the CBED patterns in Figs. 4 and 5 were taken from. The indexing was chosen to $[\bar{1}\bar{1}1]$ as can be seen from the inset. (b) Sketched configuration with indexed domain walls. For the inclined domain walls with tracks along [011], two planes are possible as shown in (c) (100) and (d) $(0\bar{1}1)$. (c) Model 1 showing the orientations of monoclinic cells in domain 3 and 2 as indexed in Figs. 4(a) and 4(b) with a (100) wall. (d) Model with domain 2 in $[0\bar{1}\bar{1}]_m$ orientation and a $(0\bar{1}1)$ wall.

The proj. WP and WP are taken from the same exposures, just the intensity of the first-order Laue zone (FOLZ) is enhanced for the WP. The mirror symmetry was checked by

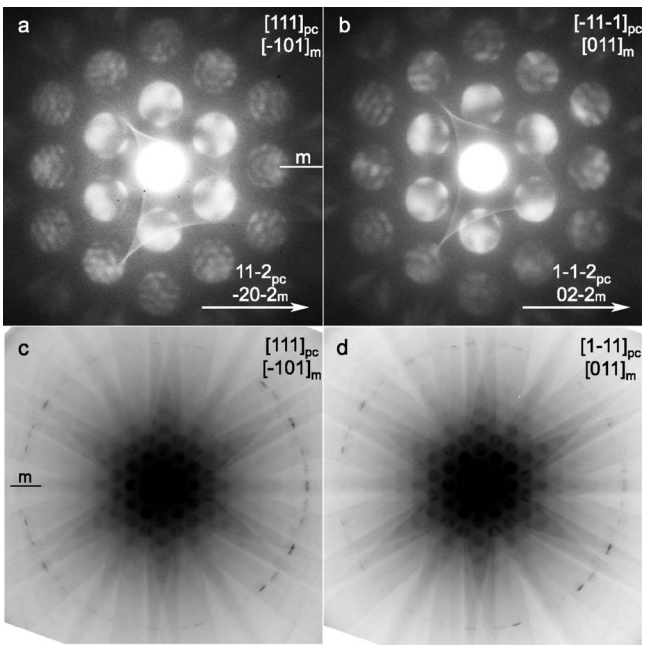

FIG. 4. Projected whole patterns (proj. $[111]_{pc}$ WPs) of domain 3(a) and domain 2(b) and whole pattern (WP) from domain 3(c) and 2(d). In (a) and (c) for domain 3(a) horizontal mirror plane is present. No symmetry is found in the patterns of domains 2(b) and 2(d).

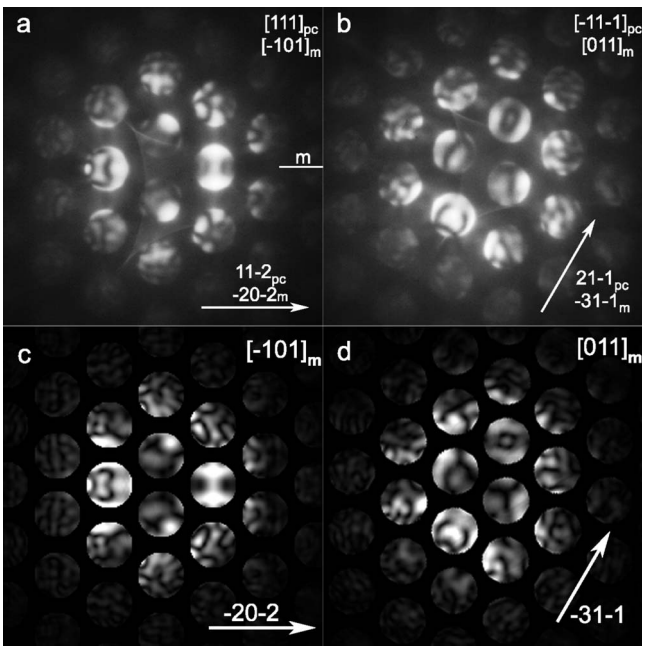

FIG. 5. The $[111]_{pc}$ dark-field patterns (DPs) of domain 3(a) and domain 2(b). The horizontal mirror plane is also found in the DP of domain 3(a). (b) The mirror expected from proj. WP of domain 2 is not found in the DP. [(c) and (d)] The orientations could be determined by comparison to simulations. Simulations were done using monoclinic structural model and 75 nm thickness for domain 3(c) and 70 nm for domain 2(d).

DPs with $11\bar{2}_{pc}$ reflections lying on the mirror plane tilted into exact Bragg conditions [Figs. 5(a) and 5(b)]. For domain 2 the most favorable orientation of a possible mirror plane from proj. WP is $(1\bar{1}0)$. In the FOLZ ring of the WP [Fig. 4(d)], one can see the different intensities that break the symmetry. This breakdown is also present in the intensity distribution of the ZOLZ reflections in the DP [Fig. 5(b)]. $\langle 111\rangle_{pc}$ type zone axes without symmetry are only present in the monoclinic structure. So the zone axis in domain 3 must be of type $\langle 101\rangle_m$, for domain 2 it has to be of type $\langle 011\rangle_m$.

The final indexing was done after comparison with simulated DPs (Ref. 25) shown in Figs. 5(c) and 5(d). For each domain all four possible zone axes with their DPs have been simulated. Because of symmetry restrictions only two dark field tilts need to be simulated for domain 3. For domain 2 all six DP tilts have to be simulated due to the missing symmetry.

The best match was observed for $[\bar{1}01]_m$ zone axis and $\bar{2}02\bar{}_m$ dark field tilt for domain 3 shown in Fig. 5(c). For domain 2, $[011]_m$ zone axis orientation with $\bar{3}1\bar{1}$ in Bragg condition shown in Fig. 5(d) matches best with the experimental pattern. Those orientations lead to a domain-wall model shown in Fig. 3(c). Both domains share a common *c* axis, but are rotated by 90°. Another possible orientation for domain 2 is $[0\bar{1}\bar{1}]_m$ with $3\bar{1}1$ in Bragg condition. This orientation together with a $(0\bar{1}1)_{pc}$ domain wall leads to a monoclinic domain-wall model that could have developed from a tetragonal tail to side configuration[26] [Fig. 3(d)].

In addition, simulations were performed using rhombohedral and tetragonal structural models. For the symmetric orientation of domain 3 the differences are less pronounced. Only for the orientation of domain 2 this produces patterns that allow a distinction between the structural models. To observe similar intensities in the BF and DP disk the beam tilt must be out of the mirror plane which is present along all $\langle 111\rangle_{pc}$ axes in both structures. The mirror plane would be parallel to the $(101)_{pc}$ plane as indexed in the inset of Fig. 3(a). From Figs. 4(b) and 4(d) it can be seen that this is not the case.

B. Heating experiment

Sample *B* was investigated at room temperature and ≈300 °C. Two grains, one with $\langle 100\rangle_{pc}$ and the other with $\langle 110\rangle_{pc}$ orientation, were chosen for the experiment. The grain with $\langle 100\rangle_{pc}$ orientation did not show domain configuration. By CBED no zone axis symmetry was found in this area as shown in Fig. 6(a) according to monoclinic structure.

In the grain with $\langle 110\rangle_{pc}$ orientation a complex domain configuration with nanodomains within microdomains was observed at room temperature (Fig. 6(e)). In some cases, a contribution of other nanodomains to the observed patterns could not be excluded. For the $[\bar{1}10]_{pc}$, ZAP shown in Fig. 6(c) there was no such evidence. The details in the pattern look clear and the ZOLZ reflections are homogeneously excited. The beam position in the corresponding double exposure in Fig. 6(e) lies also within one nanodomain of approximately 30 nm width. This was checked by small beam shifts which did not result in a change of the pattern. Since both monoclinic and rhombohedral structures have $\langle 110\rangle_{pc}$ orientations without symmetry, only tetragonal symmetry can be excluded. Corresponding to the other results in this report the monoclinic model is favored.

At 300 °C, tetragonal symmetry was observed in both grains. The $(010)_t$ mirror is present in the $[100]_t$ ZAP [Fig. 6(b)] and the tilted $[101]_t$ pattern [Fig. 6(d)]. The nanodomains in the complex domain configuration in the $[\bar{1}10]_{pc}$ grain had disappeared at 300 °C. The microdomains now look very uniform and can be described by tetragonal 90° domains with one domain oriented along $[101]_t$ and the next domain oriented along $[110]_t$. The tracks of the inclined domain walls run in $[11\bar{1}]_{pc}$ direction. Splitting of reflections in Selected Area Diffraction (SAD) was not observed. This can be attributed to the small $\frac{c}{a}$ ratio at this temperature. The change in domain structure is pointed out by the double exposures in Figs. 6(e) and 6(f).

IV. DISCUSSION

CBED is sensitive to little distortions in crystals. The probed volume is small, defined by spot size and sample thickness. So crystal symmetry can be determined on a local scale. The volume must be free of defects. In PZT, the most prominent defects are domain walls. They can be recognized in TEM imaging so one can pick a single domain for diffraction. For morphotropic PZT, the domain structures are less clear. Nanodomains occur, domain walls can be observed out of the {101} and {100} planes.[28] So finding defect free volumes becomes more difficult.

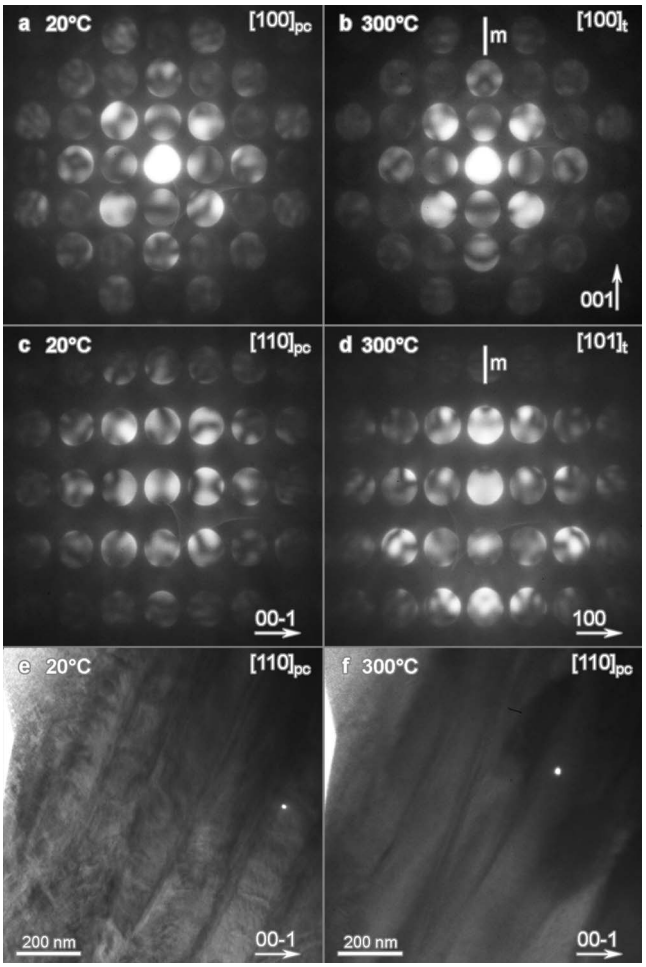

FIG. 6. (a) The $[100]_{pc}$ ZAP at 20 °C and (b) ≈300° taken from an area without domain contrast point out the change in symmetry. No symmetry was found at room temperature while a $(010)_t$ mirror is present at ≈300 °C. (c) The $[110]_{pc}$ ZAP of a nanodomain at room temperature shows no symmetry. (d) In the tilted pattern of the neighboring domain at ≈300 °C, a $(010)_t$ mirror plane is present. The double exposures (e) and (f) reveal the disappearance of nanodomains with increasing temperature and the beam positions for the $[110]_{pc}$ patterns in (c) and (d).

We used a LaB_6 cathode and spot size of 10 nm in this work and the specimen thickness suitable for symmetry determination at 100 kV lies in the range from 50 to 100 nm. So the probed volume is limited to a minimum of 4000 nm^3 or approximately 60,000 unit cells.

The results obtained under these conditions can be well described with monoclinic and tetragonal structural models, if a homogeneous crystal structure within the investigated domains is assumed. The observation of tetragonal symmetry at 300 °C and the $(110)_{pc}$ mirror plane neighboring domains justify this assumption.

This on the other hand requires the assumption that the structure does not change between neighboring domains. This might be inadequate considering possible coexistence of the F_M and F_T phase due to x-ray diffraction (XRD) results[14] and previous CBED results of the same composition, where

tetragonal symmetry was also observed at room temperature.[29,21] But the monoclinic model by Noheda *et al.*[4] seems to apply quite well to the average structure within the probed volume as pointed out by the simulated DP matching well to the experimental ones. Even the cell orientations can be derived by comparison of simulated patterns with observed ones. The model with parallel *c* axis in both domains and (100) domain wall is favored because it can evolve out of a single tetragonal domain and is uncharged.

The heating experiment proved that areas which are monoclinic at room temperature transform from F_M to F_T by a change in CBED symmetry. The nanodomains within microdomains present at room temperature disappear and only microdomains are present at 300 °C that reveal zone axis symmetry according to tetragonal structure. This change in domain structure has already been observed by Asada *et al.*[30] in a $PbZr_{0.53}Ti_{0.47}O_3$. In their nomination the domain structure containing nanodomains at room temperature is called monoclinic type I. They observed another domain structure in PZT called monoclinic type II.[30] This matches with our observations, because we also observed monoclinic symmetry in wider domains in sample *A* and sample *B*. The different domain sizes can be related to domain growth or, respectively, ordering of lead displacements.[6] The various domain configurations may impede a prediction of the crystal symmetry just by domain contrast. But even with CBED we are restricted by spot size and specimen thickness and some areas might be excluded from examination.[28]

Grinberg *et al.*[31] predicted different polarization directions for each unit cell within a $4\times2\times1$ supercell. They showed that the atomic displacements vary dependent on the local arrangement of B cations. Experimental evidence that the local structure may vary from the averaged one was given for example by Dmowski *et al.*[32] An experiment performed by us with the rhombohedral composition $PbZr_{0.60}Ti_{0.40}O_3$ on a Jeol 2010FEF (Ref. 33), with field-emission gun and Ω-energy filter using a spot size of 1 nm, did not reveal a time stable symmetric intensity distribution within the pattern. This was the same sample position, which produced a mirror symmetry in $\langle 111\rangle_{pc}$ pattern recorded using a spot size of 10 nm of a LaB_6 cathode. It has to be noted, that a ten times smaller spot size decreases the investigated volume by a factor of $\frac{1}{100}$. Thus only few columns of atoms contribute to the CBED pattern. So a small instability of the beam has a considerable influence on the volume probed. Therefore the intensity distribution in the pattern may change according to the atomic displacements present. This influence is reduced by a larger spot size. The averaging over more atomic positions leads to a higher apparent symmetry combined with an increase in the anisotropic displacement parameters (ADP).[6] Despite the larger spot size we gained no evidence, that the local symmetry is higher than monoclinic. Therefore our findings are in good agreement with the x-ray diffraction patterns of the same material[14] and those by Noheda *et al.*[7] They also match within the experimental error of the composition to the findings by Souza Filho *et al.*[9] Furthermore we provided direct evidence that the nanodomains are formed due to the reduction to monoclinic symmetry, what was still discussed concerning the interpretation of x-ray diffraction patterns.[14,12]

V. CONCLUSION

Due to the breakdown of zone axis symmetry in CBED patterns of some domains and the presence of a $\{110\}_{pc}$ in other domain, the average crystal symmetry in the probed volume of about 60000 unit cells has to be monoclinic. The orientation relationship of domains can be derived from simulated DP patterns. A F_M to F_T phase transition was observed with increasing temperature. This was accompanied by disappearance of nanodomains within tetragonal microdomains. Therefore these nanodomains are attributed to be a result of the F_T to F_M transition upon cooling. Nevertheless monoclinic symmetry may not exist in nanodomains only, this symmetry was observed in domains with widths of about 100 nm as well. This makes the monoclinic structure detectable by x rays with a coherence length of ≈100 nm.[6] In volumes smaller than 10 nm width, CBED examination was not feasible. On that scale the symmetry is most likely expected to be monoclinic or lower.

ACKNOWLEDGMENTS

Financial support was provided by the Sonderforschungsbereich 595 of the Deutsche Forschungsgemeinschaft. Special thanks go to Hans Kungl and Michael J. Hoffman for providing the material. The work at Terauchi Laboratory in the Institute of Multidisciplinary Research for Advanced Materials (IMRAM) at Tohoku University, Sendai, Japan was funded by the Japan Society for the Promotion of Science (JSPS). The authors want to thank F. Satou for great help with TEM-sample preparation, all members of the Terauchi Laboratory for their hospitality, the colleagues in Darmstadt, J. Kling, L. Schmitt, and K. A. Schönau for helpful discussions.

*schierholz@st.tu-darmstadt.de

[1] M. J. Hoffmann, M. Hammer, A. Endriss, and D. C. Lupascu, Acta Mater. **49**, 1301 (2001).
[2] W. R. Jaffe, B. Cook, and H. Jaffe, *Piezoelectric Ceramics* (Academic, New York, 1971).
[3] S. K. Mishra, D. Pandey, and P. S. Singh, Appl. Phys. Lett. **69**, 1707 (1996).
[4] B. Noheda, J. A. Gonzalo, L. E. Cross, R. Guo, S.-E. Park, D. E. Cox, and G. Shirane, Phys. Rev. B **61**, 8687 (2000).
[5] D. L. Corker, A. M. Glazer, R. W. Whatmore, A. Stallard, and F. Fauth, J. Phys.: Condens. Matter **10**, 6251 (1998).
[6] A. M. Glazer, P. A. Thomas, K. Z. Baba-Kishi, G. K. H. Pang, and C. W. Tai, Phys. Rev. B **70**, 184123 (2004).
[7] B. Noheda, D. E. Cox, G. Shirane, R. Guo, B. Jones, and L. E. Cross, Phys. Rev. B **63**, 014103 (2000).
[8] K. C. V. Lima, A. G. Souza Filho, A. P. Ayala, J. Mendes Filho,

P. T. C. Freire, F. E. A. Melo, E. B. Arau'jo, and J. A. Eiras, Phys. Rev. B **63**, 184105 (2001).
[9] A. G. Souza Filho, K. C. V. Lima, A. P. Ayala, I. Guedes, P. T. C. Freire, F. E. A. Melo, J. Mendes Filho, E. B. Araujo, and J. E. Eiras, Phys. Rev. B **66**, 132107 (2002).
[10] D. Pandey and Ragini, Z. Kristallogr. **218**, 1 (2003).
[11] A. K. Singh, D. Pandey, S. Yoon, S. Baik, and N. Shin, Appl. Phys. Lett. **91**, 192904 (2007).
[12] L. A. Schmitt, K. A. Schönau, R. Theissmann, H. Fuess, H. Kungl, and M. J. Hoffmann, J. Appl. Phys. **101**, 074107 (2007).
[13] B. Noheda, D. E. Cox, G. Shirane, J. Gonzalo, L. Cross, and S. Park, Appl. Phys. Lett. **74**, 2059 (1999).
[14] K. A. Schönau, L. A. Schmitt, M. Knapp, H. Fuess, Rüdiger-A. Eichel, H. Kungl, and M. J. Hoffmann, Phys. Rev. B **75**, 184117 (2007).
[15] Y. U. Wang, Phys. Rev. B **74**, 104109 (2006).
[16] Y. U. Wang, Phys. Rev. B **76**, 024108 (2007).
[17] D. Vanderbilt and M. H. Cohen, Phys. Rev. B **63**, 094108 (2001).
[18] Y. U. Wang, Phys. Rev. B **73**, 014113 (2006).
[19] A. K. Singh and D. Pandey, Phys. Rev. B **67**, 064102 (2003).
[20] H. Wang, J. Zhu, N. Lu, A. A. Bokov, Z.-G. Ye, and X. W. Zhang, Appl. Phys. Lett. **89**, 042908 (2006).
[21] R. Theissmann, L. Schmitt, J. Kling, R. Schierholz, K. A. Schönau, and H. Fuess, J. Appl. Phys. **102**, 024111 (2007).
[22] K. A. Schönau, M. Knapp, H. Kungl, M. J. Hoffmann, and H. Fuess, Phys. Rev. B **76**, 144112 (2007).
[23] M. Hammer and M. J. Hoffmann, J. Am. Ceram. Soc. **81**, 3277 (1998).
[24] A. Yasuhara, JEOL News, Electron Opt. Instrum. **40**, 46 (2005).
[25] K. Tsuda and M. Tanaka, Acta Crystallogr., Sect. A: Found. Crystallogr. **55**, 939 (1999).
[26] Y. H. Hu, H. M. Chan, Z. X. Wen, and M. P. Harmer, J. Am. Ceram. Soc. **69**, 594 (1986).
[27] J. Sapriel, Phys. Rev. B **12**, 5128 (1975).
[28] I. M. Reaney, J. Electroceram. **10**, 10832 (2006).
[29] R. Schierholz, Acta Crystallogr., Sect. A: Found. Crystallogr. **61**, C400 (2005).
[30] T. Asada and Y. Koyama, Phys. Rev. B **75**, 214111 (2007).
[31] I. Grinberg, V. R. Cooper, and A. M. Rappe, Phys. Rev. B **69**, 144118 (2004).
[32] W. Dmowski, T. Egami, L. Farber, and P. K. Davies, *Fundamental Physics of Ferroelectrics*, AIP Conf. Proc. No. 582 (AIP, New York, 2001), p. 33.
[33] M. Tanaka, K. Tsuda, M. Terauchi, K. Tsuno, T. Kaneyama, T. Honda, and M. Ishida, J. Microsc. **194**, 219 (1999).